Int. J. Heat Mass Transfer. Vol. 36, No. 9, pp. 2281–2292, 1993
Printed in Great Britain

0017-9310/93 $6.00 + 0.00

An analysis of the combined conductive–radiative heat transfer between a surface and a gas-fluidized bed at high temperature

HAMDY M. SHAFEY, A. M. ABD EL-GHANY and A. M. NASSIB
Department of Mechanical Engineering, Assiut University, Assiut, Egypt

(*Received* 21 *May* 1992 *and in final form* 23 *November* 1992)

Abstract—A theoretical investigation of the combined conductive radiative wall-to-fluidized bed heat transfer is presented. The packet of emulsion is assumed to be an absorbing, emitting, and scattering nongray medium. Equations of energy and radiative transfer in the packet are solved simultaneously using an iterative numerical method. The bubble is modelled as a hemisphere of gas enclosed by the emulsion and the nongray heat transfer surface. Heat transfer coefficients were calculated for different bed systems in the temperature range 300–1000 C. The predictions by the present analysis were in good agreement with available experimental data. The radiative contribution of as much as 35% varies directly with bed temperature, particle size and emissivity, surface temperature and emissivity. Both isotropic scattering and gray medium approximations were found to be acceptable for practical applications.

1. INTRODUCTION

FLUIDIZED bed technology offers an attractive way of combustion of even low grade fuels such as coals and solid wastes, with clean exhaust gases to the environment. Increased heat transfer rates to tubes immersed in the fluidized bed yield smaller combustor and boiler sizes. Also, fluidized-bed furnaces with excellent heat transfer coefficients and uniform bed temperatures should offer a new tool to handle heat treatment and powder sintering processes in metallurgical industries. In spite of the existing information in the literature [1–3] on fluidized bed heat transfer, the designer of a fluidized-bed combustor or furnace faces many uncertainties, especially the contribution of thermal radiation at high temperatures. In the last two decades, several investigators [4–14] have devoted their efforts to approach an accurate estimate of this contribution. Theoretical analyses were based on the gas film-packet theory [2, 3], for small particles up to 1.5 mm in diameter. On the other hand, the results of experimental research works [12–14] were limited to certain conditions and characteristics of the bed and cannot be extended or correlated to the general applications. A brief review of the available theoretical analyses is given below.

Vedamurthy and Sastri [4], Thring [6] and Zhang *et al.* [9] considered the gas film-packet theory and treated the packet of emulsion as blackbody layers radiating to a black surface, while they assumed that the gas film is transparent. Kolar *et al.* [8] used an alternate-slab model with a numerical technique and treated the particles and the gas in the emulsion as gray solid slabs separated by transparent gas and radiating to each other. They concluded that the thickness of the gas film adjacent to the heat transfer surface controls the radiative contribution. An arbitrary value of this thickness of 0.08 of the particle diameter d_p was found satisfactory to have a good agreement with experimental results [8]. Yoshida *et al.* [5] obtained an expression for the bubble radiative contribution, by considering the bubble as a half sphere surrounded by black bed and residing on a gray surface. An estimate of this contribution was found to be from 1 to 5% of the overall heat transfer coefficient for bed temperatures from 500 to 1500 C [5]. Bhattacharya and Harrison [7] improved the analysis carried out by Vedamurthy and Sastri [4] by treating the emulsion as an absorbing, emitting gray medium exchanging radiation with a black surface. A more realistic model was proposed by Flamant and Arnaud [10] in which they treated the packet of emulsion as an optically thick, absorbing, emitting and gray medium. They applied Rosseland approximation [10] to simply express the radiative flux as a function of the local temperature. Flamant and Menigault [11] extended the previous analysis [10] to the practical application of fluidized bed combustion for which the bubbles are composed of a gray dispersion of fine particles in an absorbing gas. Their results [11] showed that at a bed temperature of 900 C the bubble radiative contribution is significant and ranges between 5 and 9% for their bed conditions.

The purpose of this paper is to formulate and solve the real problem of simultaneous one-dimensional heat transfer by conduction and thermal radiation between an atmospheric fluidized bed and a surface of a stationary wall. The analysis is based on the two-phase theory and a gas film-packet model. Both the residence time for emulsion packet and the bubble

NOMENCLATURE

Ar Archimedes number, $gd_p^3\rho_g(\rho_s-\rho_g)/\mu_g^2$
a_l coefficient in equation (14)
b_{iz} elements of the eigenvectors in equation (16)
C_e effective specific heat of the emulsion phase [J kg^{-1} K^{-1}]
C_s specific heat of the solid bed material [J kg^{-1} K^{-1}]
d_p particle diameter [m]
d_t tube diameter [m]
$e_{\lambda,b}$ spectral blackbody emissive power [W m^{-2} μm^{-1}]
$F_{0\lambda}$ fractional blackbody emissive power in range 0–λ
f_o fraction of time the gas bubble is in contact with the heat transfer surface
G_1, G_2 constants of integration in equation (20)
g gravitational acceleration [m s^{-2}]
g_α constants of integration in equation (16)
h_c conductive contribution of the overall heat transfer coefficient [W m^{-2} K^{-1}]
h_{cc}, h_{rc} conductive and radiative heat transfer coefficients, respectively, for the packet only [W m^{-2} K^{-1}]
h_{ov} overall bed-to-surface heat transfer coefficient [W m^{-2} K^{-1}]
h_{rb} radiative heat transfer coefficient for the bubble only [W m^{-2} K^{-1}]
h_{rt} total bed-to-surface radiative heat transfer coefficient [W m^{-2} K^{-1}]
$I(\tau, \mu)$ local spectral diffuse radiation intensity at optical depth τ in the packet for a direction μ [W m^{-2} μm^{-1} sr^{-1}]
$I_b(\tau)$ local spectral blackbody radiation intensity at an optical depth τ in the packet [W m^{-2} μm^{-1} sr^{-1}]
$I_{b,w}$ spectral blackbody radiation intensity calculated at surface temperature [W m^{-2} μm^{-1} sr^{-1}]
K_s, K_t bulk spectral scattering and extinction coefficients, respectively, of the packet layer [m^{-1}]
k_e effective thermal conductivity of the emulsion [W m^{-1} K^{-1}]
k_g, k_s thermal conductivity of the fluidizing gas and solid bed material, respectively [W m^{-1} K^{-1}]
L_e effective thickness of the packet [m]
L_g gas-film thickness [m]
$p(\mu, \mu')$ azimuthally averaged scattering phase function
$q_c(x)$ instantaneous local conductive flux [W m^{-2}]
$q_r(x)$ instantaneous local radiative flux [W m^{-2}]
q_{rb} bubble phase radiative flux [W m^{-2}]
s_{il} constants of the particular solution in equation (16)
$T(x, t)$ local instantaneous temperature in the emulsion packet [°C, K]
T_b bed temperature [°C, K]
T_w surface temperature [°C, K]
t time [s]
t_r residence time [s]
U gas fluidizing velocity [m s^{-1}]
U_{mf} minimum fluidization velocity [m s^{-1}]
v volume concentration of the particles in the emulsion phase
W fluidization number, U/U_{mf}
w_j Gaussian weights.

Greek symbols

α particle size parameter, $\pi d_p/\lambda$
α_e effective diffusivity of the emulsion packet [m^2 s^{-1}]
γ_α eigenvalues in equation (16)
ε_e effective spectral hemispherical emissivity of the emulsion phase
ε_{mf} bed voidage at minimum fluidization
ε_p, ε_w spectral hemispherical emissivities of a bed particle and the heat transfer surface, respectively
Θ scattering angle [rad]
θ polar angle [rad]
λ wavelength in the vacuum [μm]
μ cos θ
μ_g viscosity of the fluidizing gas [N s m^{-2}]
μ_j Gaussian divisions
ν discrete order of the time instant
ρ_e effective density of the emulsion phase [kg m^{-3}]
ρ_g, ρ_s densities of the fluidizing gas and the solid bed material, respectively [kg m^{-3}]
ρ_w spectral hemispherical reflectivity of the heat transfer surface
τ optical depth
τ_l optical thickness of the packet layer
Φ_s sphericity of the bed particles
ψ azimuthal angle [rad]
$\tilde{\omega}$ spectral scattering albedo of the packet layer.

frequency are functions of the fluidization conditions. An energy equation is used to account for the coupled transient conductive–radiative heat transfer within the emulsion packet while coming in contact with the gas film. The local radiative flux divergence term is obtained by solving the integro–differential equation of the radiative transfer in the absorbing, emitting and anisotropically scattering nongray medium of the packet layer. Both energy and radiative transfer equations are solved simultaneously using an iterative method and a numerical technique. The resulting instantaneous temperature distribution within the packet together with the radiative flux in the bubble phase are analyzed to estimate average bed-to-surface heat transfer coefficients at different conditions. The results of the present analysis were compared with the experimental results available in the literature. The effects of the bed particle size and emissivity, bed temperature, fluidizing velocity and surface reflectivity and temperature on the radiative and overall heat transfer coefficients are investigated. Approximate solutions dealing with scattering and gray medium assumptions are also investigated.

2. THEORETICAL ANALYSIS

When a bed of solid particles is fluidized by a gas, the minimum bubbling gas velocity is usually exceeded and bubbles of the gas are thus formed and rise through the entire fluidized bed. The bed particles are mixed violently and it is seen as bulks of emulsion vigorously bubbling. Such a bed is called a bubbling fluidized bed. The heat transfer process between surfaces and a bubbling fluidized bed of small particles ($d_p \leqslant 1$ mm) can be well understood and modelled on the base of the gas film-packet hydrodynamic model where convection is neglected due to small gas velocities. The present analysis will be as follows.

2.1. *Theoretical model and assumptions*

Figure 1 shows the important features of the heat transfer model chosen for the present study. The heat transfer surface having a constant temperature T_w is treated as a diffused surface characterized by a spectral hemispherical reflectivity ρ_w ($= 1 - \varepsilon_w$) which depends on the surface material and conditions. The reflectivity, ρ_w is usually a function of the radiation wavelength and surface temperature. A stationary thin layer of the fluidizing gas (gas film) is always adjacent to the surface. The value of the thickness L_g of this layer depends on the hydrodynamic conditions of the fluidized bed and an optimum value of which was found to be $L_g = 0.08\ d_p$ [6, 8]. The gas film may be treated with varying linear temperature distribution. Packets of emulsion come from the core of the bed at bed temperature T_b to reside on the gas film, each during an interval of time defined as the residence time t_r. A packet consists of a dispersed medium of small particles in the fluidizing gas at minimum fluidization conditions. For a well-mixed bed of particles of low Biot number ($Bi < 0.1$), negligible temperature gradients will be set up within the particles and the gas and solid phases can be assumed to be in thermal equilibrium. Practical applications of a gas-fluidized bed of small particles at high temperature, usually include bed materials (stones, ceramics, metals and its alloys) with $\rho_s = 2000$–$9000\ \mathrm{kg\,m^{-3}}$ and $k_s = 1.0$–$80.0\ \mathrm{W\,m^{-1}\,K^{-1}}$. For these situations the condition of $Bi < 0.1$ is confirmed, and the gas and particles in the packet are assumed to be at the same temperature. The thick packet can be treated by a plane-parallel layer of finite effective thickness L_e, usually taken as few times the particle size ($L_e = 3 \sim 5\ d_p$) [4, 6]. Unsteady conductive–radiative heat transfer through the packet will occur during the residence time. Then the packet with an average temperature different from T_b is swept away and replaced by a fresh one from the main region of the bed. This occurs frequently for steady bed conditions with a constant average relative frequency. The gas bubble is simply represented by a hemisphere whose base is in contact with the surface within a time fraction f_o and is surrounded by the emulsion at T_b. The bubble is assumed to contribute to the radiative heat transfer to the surface while the conduction through it is neglected. The following main assumptions are taken into consideration in the formulation of the coupled energy and radiative transfer equations in the packet layer.

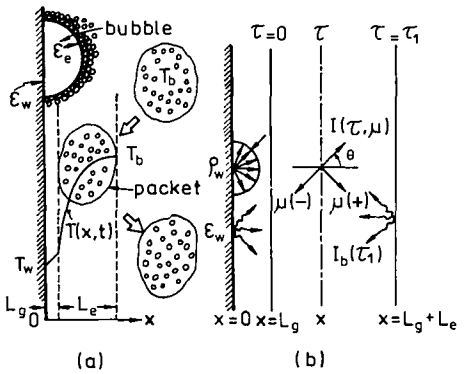

FIG. 1. Heat transfer model: (a) the physical model; (b) the radiative transfer model.

(1) The packet medium is nongray, absorbing, emitting and anisotropically scattering.
(2) The packet layer is homogeneous with uniform voidage.
(3) The entire fluidized bed is at steady state conditions.
(4) Both conduction and radiation transfer are one-dimensional.
(5) There is no heat generation source other than emission inside the packet layer.
(6) The fluidizing gas is nonemitting, nonabsorbing, with unit refractive index.

Assumptions 5 and 6 represent a simple approximation for combustion and chemical reaction pro-

cesses where heat generation occurs and participating (absorbing emitting) gases such as CO_2 and H_2O exist. It is not a difficult task to extend the present analysis to these processes. However, an accurate treatment requires precise information about types and concentrations of participating gases and size distribution of fuel or reacting particles in the emulsion phase. Presently these parameters are expected to be complicated functions of the process input data as the composition, feed rate and size distribution of the fuel, excess air ratio, bed temperature, etc.

2.2. *Basic equations for the packet of emulsion*

The three-dimensional energy equation for the transient conductive-radiative system of the packet may be written as

$$\rho_e C_e \frac{\partial T}{\partial t} + \nabla(q_c + q_r) = 0 \tag{1}$$

where q_c and q_r are the conductive and radiative fluxes respectively. Substituting for

$$q_c(x) = -k_e \frac{\partial T}{\partial x}$$

in the present one-dimensional model with k_e = constant equation (1) becomes

$$\frac{\partial^2 T}{\partial x^2} - \frac{1}{k_e}\frac{\partial}{\partial x}(q_r(x)) = \frac{1}{\alpha_e}\frac{\partial T}{\partial t} \tag{2}$$

where k_e and α_e are the effective thermal conductivity and diffusivity of the emulsion packet, respectively. The instantaneous local integrated radiative flux $q_r(x)$ is given in terms of the local spectral radiation intensity by

$$q_r(x) = \int_0^\infty \left[2\pi \int_{-1}^{1} I(x,\mu)\mu \, d\mu\right] d\lambda \tag{3}$$

where $\mu = \cos\theta$ and θ is the polar angle.

The initial condition associated with the energy equation, equation (2) is given by

$$T(x,0) = T_b, \quad (L_g \leqslant x \leqslant L_e). \tag{4}$$

Considering the energy balance at the gas film-packet interface ($x = L_g$), the corresponding boundary conditions are given by

$$T(L_g + L_e, t) = T_b, \quad t > 0 \tag{5}$$

$$k_e \frac{\partial T}{\partial x}\bigg|_{x=L_g} = k_g[T(L_g,t) - T_w]/L_g \tag{6}$$

where k_g is the thermal conductivity of the gas film calculated at a mean temperature $(T_b + T_w)/2$. The monochromatic radiation intensity $I(x,\mu)$ in equation (3) can be found by solving the following quasi-steady transfer equation [15] written for azimuthally symmetric radiation field in the packet layer.

$$\mu \frac{dI(\tau,\mu)}{d\tau} = -I(\tau,\mu) + \frac{\tilde{\omega}}{2}\int_{-1}^{1} p(\mu,\mu')I(\tau,\mu')\,d\mu' + (1-\tilde{\omega})I_b(\tau) \tag{7}$$

where $p(\mu, \mu')$ is the azimuthally averaged scattering phase function and $\tilde{\omega}$ is the spectral scattering albedo of the packet layer defined by

$$\tilde{\omega} = K_s/K_t. \tag{8}$$

In equation (7) the ordinate x is replaced by the optical depth τ defined by

$$\tau = K_t(x - L_g) \tag{9}$$

where K_s and K_t are the bulk spectral scattering and extinction coefficients of the packet layer, respectively.

The local spectral intensity of a blackbody radiation in a vacuum is given in terms of the local temperature $T(\tau)$ by the Planck distribution as

$$I_b(\tau) = 2C_1\lambda^{-5}/\{\exp[C_2/\lambda T(\tau)] - 1\} \tag{10}$$

where C_1 and C_2 are known constants [16].

The boundary conditions associated with the radiation transfer equation equation (7) are expressed as follows. For the nonabsorbing gas film the reflection–emission condition at the surface ($x = 0$) exactly applies at the packet layer boundary ($\tau = 0$) and is given by

$$I(0,\mu) = 2\rho_w \int_0^1 I(0,-\mu)\mu\,d\mu + \varepsilon_w I_{b,w}, \quad (0 < \mu \leqslant 1) \tag{11}$$

where $I_{b,w}$ is the spectral blackbody radiation intensity calculated at the surface temperature T_w. The other boundary condition may be given by

$$I(\tau_1, -\mu) = I_b(\tau_1), \quad (0 < \mu \leqslant 1) \tag{12}$$

where $\tau_1 = K_t L_c$ is the optical thickness of the packet layer.

2.3. *Solution method for the packet*

It is quite difficult to find a closed form analytical solution of the coupled equations of energy and radiative transfer, equations (2) and (7). A first step to approach the solution of both equations (2) and (7) is to treat the variation with the time t and the cosine variable μ in numerical manner. Thus substituting for the differentiation with respect to t in equation (2) and the integration with respect to μ in equation (7) by their approximate numerical form. Dividing the residence time t_r into M equal small increments of time Δt and using a backward finite difference formula for the derivative $\partial T/\partial t$ equation (2) may be rewritten in a semi-numerical form as

$$\frac{d^2T^{(\nu)}(x)}{dx^2} - \frac{1}{k_e}\frac{d}{dx}(q_r^{(\nu)}(x)) = \frac{1}{\alpha_e}\frac{[T^{(\nu)}(x) - T^{(\nu-1)}(x)]}{\Delta t}, \quad (\nu = 1,2,\ldots,M) \tag{13}$$

where $T^{(\nu)}(x)$ is the temperature distribution in the

packet layer at a time instant of order (v). The initial condition equation (4) will be considered as an initial temperature distribution $T^{(0)}(x) = T_b$. The integration in equation (7) can be replaced by Gaussian quadrature formula [15] in the nth approximation if the continuous ordinate $1 \geqslant \mu \geqslant -1$ is replaced by the Gaussian division $\mu_i (i = 1, 2, \ldots, 2n)$. Moreover the blackbody intensity $I_b(\tau)$ is expressed as a power series

$$I_b(\tau) = \sum_{l=0}^{m} a_l \left(\frac{\tau}{\tau_1}\right)^l. \tag{14}$$

Thus equation (7) may be written in the discrete ordinate form

$$\mu_i \frac{dI(\tau, \mu_i)}{d\tau} = -I(\tau, \mu_i) + \frac{\tilde{\omega}}{2} \sum_{j=1}^{2n} w_j p(\mu_i, \mu_j) I(\tau, \mu_j) + (1-\tilde{\omega}) \sum_{l=0}^{m} a_l \left(\frac{\tau}{\tau_1}\right)^l, \quad (i = 1, 2, \ldots, 2n) \tag{15}$$

where w_j ($j = 1, 2, \ldots, 2n$) are the Gaussian weights. The number of terms m and the coefficients a_l in equation (14) are dependent on the wavelength λ, and they are determined within an arbitrary degree of accuracy by the following procedure. The interval from 0 to 1 for (τ/τ_1) is divided into known number of divisions (e.g. 20) and then the numerical values of temperature corresponding to these divisions are obtained from the known function $T^{(v)}(\tau)$. Numerical values of $I_b(\tau)$ are obtained by substituting the numerical values of the temperature and the specified wavelength in equation (10). Applying a least square method, the m coefficients a_l are obtained. The solution of the system of equations equation (15) for a known temperature distribution is given by [17]

$$I(\tau, \mu_i) = \sum_{\alpha_-} g_\alpha b_{i\alpha} \exp[\gamma_\alpha \tau] + \sum_{\alpha_+} g_\alpha b_{i\alpha} \exp[\gamma_\alpha (\tau - \tau_1)] + \sum_{l=0}^{m} s_{il} (\tau/\tau_1)^l, \quad (i = 1, 2, \ldots, 2n) \tag{16}$$

where γ_α and $b_{i\alpha}$ are the eigenvalues and the eigenvectors for the complementary solution corresponding to the homogeneous $2n$ coupled equations equation (15) [17], and α_- and α_+ mean the summations over the negative and positive values of γ_α, respectively. The constants s_{il} for the particular solution are obtained by applying the Gaussian elimination method corresponding to the non-homogeneous term in equation (15). The constants of integration g_α are obtained by applying the boundary conditions equations (11) and (12) in their discrete ordinate form given by

$$I(0, \mu_i) = 2\rho_w \sum_{j=n+1}^{2n} w_j |\mu_j| I(0, \mu_j) + \varepsilon_w I_{b,w}, \quad (i = 1, 2, \ldots, n) \tag{17}$$

$$I(\tau_1, \mu_i) = I_b(\tau_1), \quad (i = n+1, \ldots, 2n). \tag{18}$$

To solve the energy equation equation (13), the radiative flux $q_r(x)$ must be obtained as a known function of x. This can be done by carrying out the integration in equation (13) with respect to both the wavelength λ and the cosine variable μ numerically as

$$q_r(x) = 2\pi \sum_{p=1}^{N} \left[\sum_{j=1}^{2n} w_j \mu_j I(x, \mu_j) \right] \Delta\lambda_p \tag{19}$$

where the whole wavelength range from 0 to ∞ is replaced with high accuracy by a finite one with N wavelength intervals $\Delta\lambda_p$. The spectral intensity $I(x, \mu_j)$ in equation (19) is given by the solution of equation (16) after substituting $\tau = K_t (x - L_g)$, where the scattering and absorption properties of the packet layer are considered constant over the interval $\Delta\lambda_p$ and calculated at the center wavelength λ_p of the interval. The energy equation equation (13) is solved using an iterative method. In this method the temperature distribution for a time instant of order v ($v = 1, 2, \ldots, M$) is assumed (usually that for the preceding instant of order $(v-1)$) to obtain the coefficients a_l of equation (14). Then the radiative transfer equation equation (16) is solved to obtain the expression of $q_r(x)$ in equation (19). Integrating equation (13) with respect to x we obtain the general expression for the temperature distribution as

$$T^{(v)}(x) = G_1 e^{Rx} + G_2 e^{-Rx} + \frac{1}{D^2 - R^2} \left[\frac{1}{k_e} \frac{d}{dx} (q^{(v)}(x)) - R^2 T^{(v-1)}(x) \right] \tag{20}$$

where

$$D = \frac{d}{dx}, \quad R = \frac{1}{[\alpha_e \Delta t]^{0.5}}.$$

The third term in the R.H.S. of equation (20) represents the particular integral solution corresponding to the terms of the preceding temperature and the divergence of the radiative flux in equation (13). For the first time instant ($v = 1$) with $T^{(0)}(x) = T_b$ = constant and keeping in mind the power and exponential functions x^l and $\exp[\gamma_\alpha x]$ found in the expression for $I(x, \mu_i)$ and by turn in $q_r(x)$, one can obtain simply the corresponding terms in the particular integral solution for any $T^{(v)}(x)$ with the appropriate constants. The new expression of $T^{(v)}(x)$ is used again to obtain new values for coefficients a_l of equation (14) and proceeding in similar manner till a final expression for $T^{(v)}(x)$ is obtained with an arbitrary chosen accuracy. Note that the expression for $T^{(v-1)}(x)$ in equation (20) is fixed for every iteration to obtain $T^{(v)}(x)$. The constants of integration G_1 and G_2 are obtained for each iteration by employing the boundary conditions equations (5) and (6).

The above procedure is repeated to obtain $T^{(v)}(x)$ for all time instants $v = 1, 2, \ldots, M$ within the residence time t_r and the corresponding radiative flux distribution $q_r^{(v)}(x)$.

2.4. *Bubble phase radiative flux*

The bubble is enclosed by only two surfaces: (1) the hemispherical diffuse nongray surface of emulsion phase having an effective spectral hemispherical emissivity ε_e and a temperature T_b, (2) the heat transfer diffuse nongray surface having a spectral hemispherical emissivity ε_w and a temperature T_w. A relation between the effective emissivity ε_e of the emulsion and the particle emissivity ε_p can be obtained by solving the equation of radiative transfer (including multiple scattering) through the optically thick dispersed medium of the emulsion with uniform hemispherical irradiation [15, 17]. Such a relation, for a bed with average voidage, is simply taken [3] as $\varepsilon_e = (\varepsilon_p)^{0.4}$. The radiant heat flux exchanged between the two surfaces through the transparent bubble for a wavelength interval $d\lambda$ may be expressed as

$$dq_{r,b} = \frac{2[e_{\lambda,b}(\lambda, T_b) - e_{\lambda,b}(\lambda, T_w)]}{\left[\frac{1}{\varepsilon_e} + \frac{2}{\varepsilon_w} - 1\right]} d\lambda. \quad (21)$$

The total radiative heat flux exchanged through the bubble is found by the integration over all wavelengths, numerically approximated as

$$q_{r,b} = 2 \sum_{p=1}^{N} \frac{[e_{\Delta\lambda_p,b}(T_b) - e_{\Delta\lambda_p,b}(T_w)]}{\left[\frac{1}{\varepsilon_e} + \frac{2}{\varepsilon_w} - 1\right]} \Delta\lambda_p \quad (22)$$

where ε_e, ε_w are mean properties calculated at the center wavelength λ_p. The arithmetic mean $e_{\Delta\lambda_p,b}$ of the blackbody emission power over the wavelength interval $\Delta\lambda_p$ for large values of $\Delta\lambda_p$ can be evaluated accurately using the blackbody function $F_{0-\lambda}$ [16] as

$$e_{\Delta\lambda_p,b}\Delta\lambda_p = \int_{\lambda}^{\lambda+\Delta\lambda_p} e_{\lambda,b}\, d\lambda = (F_{0-(\lambda+\Delta\lambda_p)} - F_{0-\lambda})\sigma T^4. \quad (23)$$

2.5. *Heat transfer coefficients*

Heat is transferred between the fluidized bed and the surface by (i) transient conduction and radiation through the emulsion phase (packet) and by (ii) radiation through the bubble phase. The time-average heat transfer coefficients for each of these processes will be denoted by h_{ce}, h_{re} and h_{rb}, respectively. The overall heat transfer coefficient, h_{ov}, may be written as

$$h_{ov} = (1 - f_o)(h_{ce} + h_{re}) + f_o h_{rb}. \quad (24)$$

The total radiative heat transfer coefficient, h_{rt} and the conductive heat transfer coefficient h_c are given by

$$\left.\begin{aligned} h_{rt} &= (1 - f_o)h_{re} + f_o h_{rb} \\ h_c &= (1 - f_o)h_{ce}. \end{aligned}\right\} \quad (25)$$

The different coefficients of heat transfer are calculated by

$$h_{ce} = \frac{1}{t_r(T_b - T_w)} \int_0^{t_r} \frac{[T(L_g, t) - T_w]}{(L_g/k_g)} dt \quad (26)$$

$$h_{re} = \frac{1}{t_r(T_b - T_w)} \int_0^{t_r} [-q_r(L_g)]\, dt \quad (27)$$

$$h_{rb} = \frac{1}{(T_b - T_w)} q_{rb}. \quad (28)$$

The integrations in equations (26) and (27) are performed numerically using the simple rectangular rule applied to the M time intervals defined before.

3. BED PARAMETERS AND PROPERTIES

3.1. *Bed parameters*

A survey of the literature has been made for the existing correlations used to determine the various bed parameters needed in the calculations for the heat transfer analysis. The following correlations were selected and employed in the present study.

(1) The minimum fluidization velocity, U_{mf}, is calculated by [18]

$$U_{mf} = \frac{\mu_g}{\rho_g d_p} \{[(27.2)^2 + 0.0408\, Ar]^{0.5} - 27.2\} \quad (29)$$

where Ar is the Archimedes number.

(2) The bed voidage, ε_{mf} at minimum fluidization is evaluated by [18]

$$\varepsilon_{mf} = (14\Phi_s)^{-1/3} \quad (30)$$

where Φ_s is the sphericity of the bed particles. For spherical particles $\Phi_s = 1$.

(3) The residence time, t_r (in seconds), is obtained by [6]

$$t_r = 8.932 \left[\frac{g d_p}{U_{mf}^2 (W-1)^2}\right]^{0.0756} \left[\frac{d_p}{0.0254}\right]^{0.5} \quad (31)$$

where $W\ (= U/U_{mf})$ is the fluidization number.

(4) The bubble time fraction f_o is determined by [6]

$$f_o = 0.08553 \left[\frac{U_{mf}^2 (W-1)^2}{g d_p}\right]^{0.1948}. \quad (32)$$

3.2. *Bed thermal properties*

High-temperature gas-fluidized beds of practical importance usually employ solid bed particles of densities much larger than the gas density ($\rho_s \gg \rho_g$). Thus the effective density ρ_e and the effective specific heat C_e of the emulsion phase can be given in terms of those of the solid bed material ρ_s and C_s, respectively, by

$$\rho_e = (1 - \varepsilon_{mf})\rho_s, \quad C_e = C_s. \quad (33)$$

The effective thermal conductivity k_e can be given by [2, 11]

$$k_c = k_g\left[1+\frac{(1-\varepsilon_{mf})(1-k_g/k_s)}{k_g/k_s+0.28\varepsilon_{mf}^{0.63}(k_g/k_s)^{0.18}}\right]. \quad (34)$$

3.3. *Bed radiative properties*

Consider that the emulsion phase is a monodispersion of large opaque spherical particles ($\Phi_s = 1$) of diameter d_p in nonabsorbing gas. Moreover the surfaces of these particles are reflecting diffusely and emitting with a spectral hemispherical emissivity ε_p. For most fluidized beds the volume concentration of the particles in the emulsion phase v ($=1-\varepsilon_{mf}$) is large ranging from 0.4 to 0.6. The particle size range for the present study $d_p = 0.1$–1.0 mm corresponds to particle size parameter range α ($=\pi d_p/\lambda$) = 5–100 (for thermal radiation wavelengths of interest). With these bed conditions the independent scattering theory can be applied and the bulk spectral scattering and extinction coefficients K_s and K_t, respectively, are determined by [19]

$$K_s = \frac{1.5}{d_p}v(1-\varepsilon_p), \quad K_t = \frac{1.5}{d_p}v. \quad (35)$$

The corresponding scattering phase function $p(\mu,\mu')$ is given by [19]

$$p(\mu,\mu') = \frac{1}{2\pi}\int_0^{2\pi}\frac{8}{3\pi}(\sin\Theta-\Theta\cos\Theta)\,d\psi' \quad (36)$$

where Θ is the scattering angle defined as

$$\cos\Theta = \mu\mu'+(1-\mu^2)(1-\mu'^2)\cos(\psi-\psi'). \quad (37)$$

The integration in equation (36) is performed numerically for each pair of $\mu = \mu_i$, $\mu' = \mu_j$ in equation (15).

4. RESULTS AND DISCUSSION

The mathematical model given in the present analysis was simulated by a computer program which has been developed and processed on the IBM XT personal computer. Values of common parameters and their divisions and intervals were chosen for accurate numerical calculations as follows. The estimated residence time t_r was divided into 5 small intervals of time variation $\Delta t = 0.08$–0.30 s depending on the bed conditions. A fixed value of the effective thickness $L_e = 5$ mm accounting for the thick packet was used with 20 equal divisions in the x direction. With surface and bed temperatures considered in the present analysis (30–1100°C), most of the blackbody radiation lies within a finite wavelength range of $\lambda = 1.0$–22.0 μm which was divided into unequal intervals. The number and values of wavelength intervals were determined mainly according to the spectral distribution of the radiative properties of the bed material. A number of 5–8 wavelength intervals was used to describe precisely the spectral variation for all materials used. Different numbers of the Gaussian divisions were checked and a value of $2n = 10$ was found to be sufficient for accurate numerical integration. The input data of the operating conditions and bed characteristics will be stated along with the figures and through the discussion of the corresponding results. The bed particles were assumed to have a sphericity $\Phi_s = 1.0$. The thermophysical properties of fluidizing gas (air), bed materials and heat transfer surfaces used in the computation were selected from various references and texts at different temperatures and wavelengths [18–24]. The temperature dependence of the emulsion properties was considered only through the parametric variation of the bed temperature, T_b.

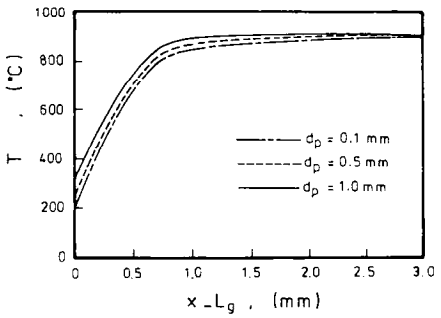

FIG. 2. Variation of temperature along emulsion at the end of residence time. Air–sand, $T_b = 900$ C, $W = 4$, oxidized copper surface, $T_w = 200$ C.

The variations of the temperature and radiative flux of the emulsion packet along its length at the end of the residence time are shown in Figs. 2 and 3, respectively. It can be seen that the temperature level increases with increase in the particle size d_p. This is due to the increase in the gas film, L_g with increase in d_p ($L_g = 0.08\,d_p$), which in turn increases the thermal conductive resistance and reduces the conductive cooling rate. The radiative flux at the surface increases with increase in d_p as shown in Fig. 3 due mainly to the decrease in the attenuation of the emitted radiation coming from the packet to the surface. This attenuation is inversely proportional to d_p as given by equation (35). It is also clear from Fig. 2 that the temperature variation is limited only to a distance of about 3 mm for all values of d_p, thus proving the validity of the boundary condition, equation (5) with the value of the effective packet thickness taken as $L_e = 5$ mm.

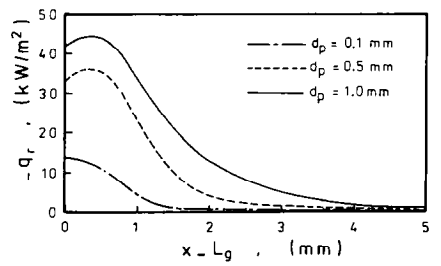

FIG. 3. Variation of radiative flux along emulsion at the end of residence time. Air–sand, $T_b = 900$°C, $W = 4$, oxidized copper surface, $T_w = 200$°C.

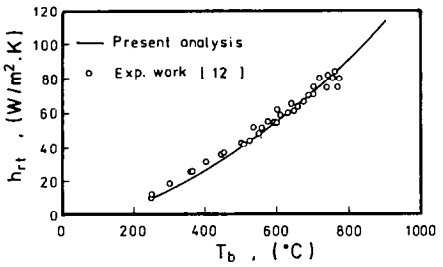

FIG. 4. Effect of bed temperature on the total radiative heat transfer coefficient. Air–sand, $d_p = 1.03$ mm, $W = 6$, $T_w = f(T_b)$.

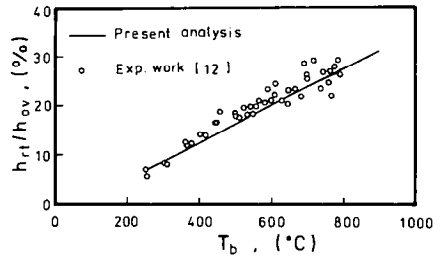

FIG. 5. Effect of bed temperature on the relative radiative contribution. Air–sand, $d_p = 1.03$ mm, $W = 6$, $T_w = f(T_b)$.

Figures 4 and 5 show the effect of T_b on the total radiative heat transfer coefficient, h_{rt} and its relative contribution, h_{rt}/h_{ov}, for an air–sand system with a fluidization number $W = 6$. The experimental results for average particle size, $d_p = 1.03$ mm presented along with the present analysis at the same conditions are of Ozkaynak *et al.* [12]. They measured the radiative heat flux using a radiometer probe whose outer window of zinc selenide served as a flat heat-transfer surface oriented vertically with average emissivity $\varepsilon_w = 0.90$. The surface temperature, T_w was varying, as a function of bed temperature, T_b, from 30 to 200°C. It is seen from Figs. 4 and 5 that the predictions by the present analysis are very close to the experimental results. In Fig. 5 the radiative contribution varies linearly from about 9 to 32% as the bed temperature increases from 300 to 900°C.

Figures 6 and 7 show the effect of the bed temperature, T_b, on the overall heat transfer coefficient,

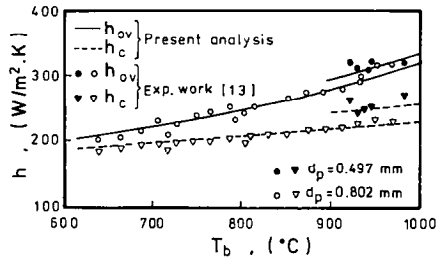

FIG. 6. Effect of bed temperature on the overall heat transfer coefficient and its conductive component. Air-residual slag of fired coal, $W = 2$, $T_w = f(T_b)$.

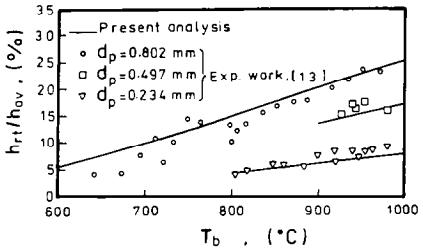

FIG. 7. Effect of bed temperature on the relative radiative contribution. Air-residual slag of fired coal, $W = 2$, $T_w = f(T_b)$.

h_{ov}, conductive component, h_c, and the relative radiative contribution, h_{rt}/h_{ov}, for residual slag of fired coal particles fluidized by air at $W = 2$. Presented also are the experimental results of Qian Renzhang *et al.* [13]. They measured the radiative contribution by an indirect method in which they deduced the conductive component, h_c, from results of cold experiment at room temperature. The high temperature bed was cooled by water flowing through a horizontal tube with outer diameter $d_t = 35$ mm. The analysis assumed the tube surface to have an emissivity ε_w which is a linear function of the bed temperature and ranging from 0.5 to 0.8. This is a good approximation for the oxidized metal of the cooling tube. The surface temperature was varying linearly with T_b from 30 to 300°C. The predictions by the present analysis almost show a good agreement with the experimental results for all particle sizes. A similar tendency as in Fig. 5 for the relative contribution of radiation can be seen in Fig. 7 except for the small values of h_{rt}/h_{ov} due to the relatively small values of particle size compared with $d_p = 1.03$ mm. This is clearly shown in Fig. 8 which shows the variation of h_{rt}/h_{ov} with the particle size d_p. The increase of h_{rt} with increase in d_p can also be understood from the discussion made before on Fig. 3. The small values of h_{rt}/h_{ov} in Fig. 7 may also be attributed to the small values of surface emissivity ($\varepsilon_w = 0.5$–0.8) compared with $\varepsilon_w = 0.9$ for the results of Fig. 5 as will be shown later.

The good agreement obtained in Figs. 6–8 in addition with previous findings [5, 6, 9], shows that

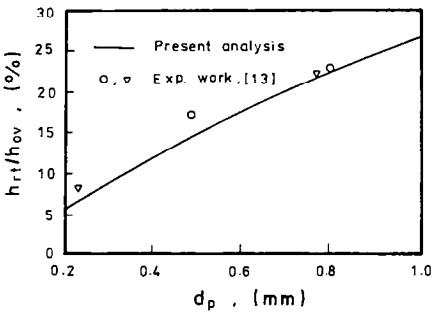

FIG. 8. Effect of particle diameter on the relative radiative contribution. Air-residual slag of fired coal, $T_b = 950$°C, $T_w = 290$°C.

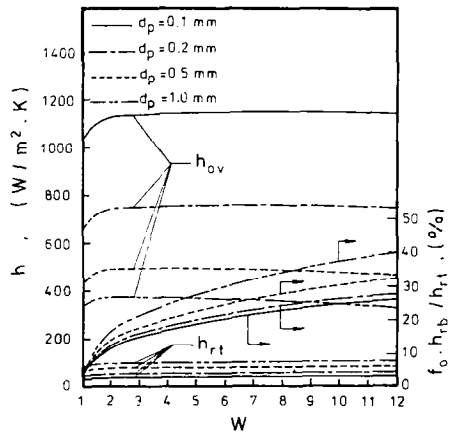

FIG. 9. Effect of fluidization number on the overall heat transfer coefficient, its radiative component and bubble contribution. Air–sand, $T_b = 900$ C, oxidized copper surface, $T_w = 200$ C.

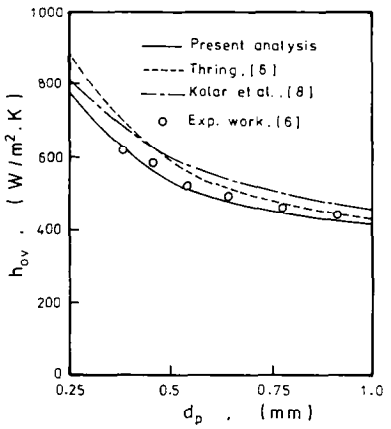

FIG. 10. Effect of particle diameter on the maximum overall heat transfer coefficient. Air–sand, $T_b = 900$ C, $W = 2$, $T_w = 30$ C.

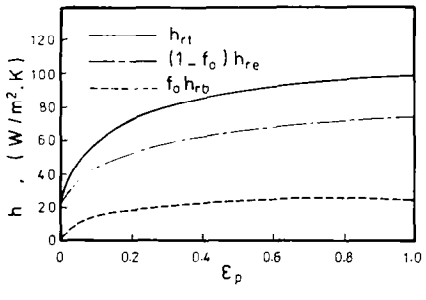

FIG. 11. Effect of particle emissivity on the radiative heat transfer coefficient, $d_p = 1.0$ mm, $T_b = 900$ C, $W = 4$, oxidized copper surface, $T_w = 200$ C.

the present one-dimensional model can be applied also to the curved surfaces of horizontal or vertical tubes with size ratios as low as: $d_t/d_p = 21$, $d_t/L_c = 4$ and $d_t/L_g = 142$ [25].

Figure 9 shows the effect of the fluidization number, W, on the overall heat transfer coefficient, h_{ov}, and its radiative component, h_{rt}, along with the radiative contribution of the bubble phase, $f_o h_{rb}/h_{rt}$, for an air–sand system. The overall coefficient increases initially with the increase in the fluidizing velocity reaching a maximum nearly at a value $W = 2$ for all particle sizes. Then it remains nearly constant and begins to slightly decrease at a value $W = 10$. The radiative component, h_{rt} increases with slow rates as W increases. However, the radiative contribution of the bubble phase increases as W increases with higher rates for $W < 2$. This is due to the increase in time during which the surface is exposed to bubbles as velocity increases. Both the radiative component and its bubble contribution increase as shown with the particle size.

The variation of maximum overall heat transfer coefficient ($W = 2$) with particle size, d_p, is presented in Fig. 10 for an air–sand system. The results of the present model are compared with the theoretical results using an alternate-slab model by Kolar *et al.* [8], and the theoretical results using a packet model by Thring [6]. Shown also for comparison are the experimental results of Broughton cited in ref. [6]. The present model and other models show the same trend. However, the predictions by the present model are in better agreement with the experimental results especially for small values of d_p at the same conditions. This may be attributed to the approximate treatment of radiation by the other two models [6, 8] as compared with the more exact one by the present model. An important observation is that the overall coefficient decreases as the particle size increases with high rates for $d_p < 0.5$ mm. This can be easily explained in view of the discussion made on Figs. 2 and 3.

Figure 11 shows the effect of varying the particle emissivity, ε_p, (for opaque particles) on the total radiative heat transfer coefficient, h_{rt} and the separate contributions due to emulsion packet, $(1 - f_o)h_{re}$, and due to bubble, $f_o h_{rb}$. The results are for an air–sand system, except the value of ε_p was varied as a parameter. The conductive coefficient h_c was found to be nearly constant ($h_c = 266$ W m^{-2} K^{-1}). All radiative coefficients increase with the increase in the particle emissivity. The total radiative coefficient is very sensitive to ε_p for highly reflecting particles. It changes from 20 W m^{-2} K^{-1} for totally reflecting particles ($\varepsilon_p = 0$) to 73 W m^{-2} K^{-1} for particles with $\varepsilon_p = 0.2$. On the other hand uncertainty in the particle emissivity value for highly emitting particles ($\varepsilon_p = 0.8$–1.0) does not lead to large errors in estimates for radiative heat transfer coefficients.

Figure 12 shows the variations of the overall heat transfer coefficient h_{ov} and its components h_c and h_{rt} with the thermal conductivity k_s of the solid bed material. The results are for an air–sand system, except the value of k_s was varied as a parameter. With values of thermal conductivity $k_s < 10$ W m^{-1} K^{-1} a noticeable effect of k_s can be found. This is because

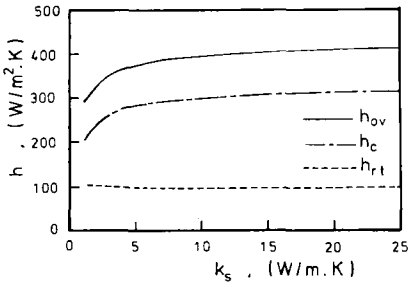

FIG. 12. Effect of thermal conductivity of bed material on the overall heat transfer coefficient and its components, $d_p = 1.0$ mm, $T_b = 900$°C, $W = 4$, oxidized copper surface, $T_w = 200$°C.

the increase in k_s decreases the packet thermal resistance and by turn decreases its relative effect on the heat transfer to the surface compared with the gas-film resistance effect. Some authors [3] found that the effect of k_s on the value of h_{ov} is modest, and they concluded that it has no effect on h_{ov}. This can be true as shown in Fig. 12 for materials of $k_s > 10$ W m^{-1} K^{-1}.

Figure 13 shows the effect of the surface temperature, T_w, on the radiative and conductive components of the overall heat transfer coefficient, h_{rt} and h_c, respectively, as predicted by the present model. Also shown are the theoretical results using alternate-slab model by Kolar *et al.* [8] and the theoretical results using a gas-film packet model developed by Bhattacharya and Harrison [7]. All results were for air–sand system with $d_p = 0.35$ mm operating at $W = 2$ and $T_b = 850$°C. The heat transfer surface was assumed to be a blackbody ($\varepsilon_w = 1$). The present model as well as the other models show the same trend of the increasing of the heat transfer coefficients with T_w. The results for h_{rt} by Bhattacharya and Harrison [7] nearly agree with the results by the present model while those by Kolar *et al.* [8] show an overestimation

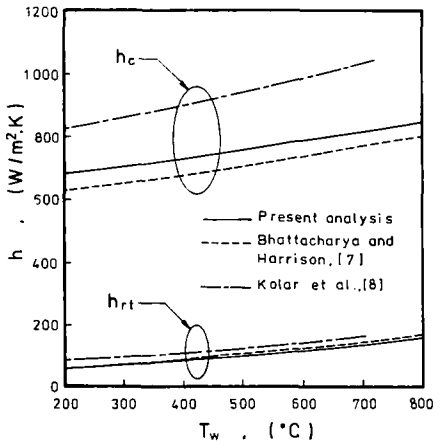

FIG. 13. Effect of surface temperature on the conductive and radiative heat transfer coefficients. Air–sand, $d_p = 0.35$ mm, $T_b = 850$°C, $W = 2$.

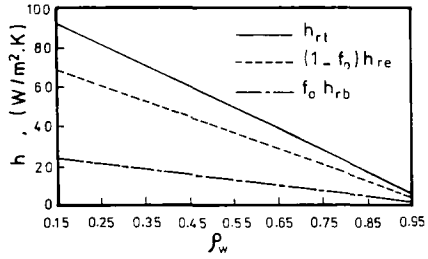

FIG. 14. Effect of surface reflectivity on the radiative heat transfer coefficients. Air–sand, $d_p = 1.0$ mm, $T_b = 900$°C, $W = 4$, $T_w = 150$°C.

from 25 to 35% as compared with the present model. However, the results for h_c show overestimation by the results of Kolar *et al.* [8] and underestimation by the results of Bhattacharya and Harrison [7]. The agreement between the results for h_{rt} by Bhattacharya and Harrison [7] and the results of the present model are due to their correct treatment of the emulsion as an absorbing and emitting but not scattering medium.

Figure 14 shows the effect of the hemispherical reflectivity, ρ_w, of the heat transfer surface on the radiative heat transfer coefficient, h_{rt}, and its components for air–sand system. The surface reflectivity was varied as a parameter rather than considering its spectral distribution for actual surface. The coefficient h_{rt} rapidly decreases by 95% as ρ_w increases from 0.15 to 0.95. Correspondingly the conductive coefficient increases by 25%. As a result, the overall coefficient was little influenced by the reflectivity of the surface ($h_{ov} = 359$–341 W m^{-2} K^{-1}). Theoretical and experimental results similar to these results were also presented by Yoshida *et al.* [5] with stainless steel pipes having reflectivity values of $\rho_w = 0.2$ (oxidized surface) and $\rho_w = 0.83$ (polished surface). The different effects of the radiative properties, ε_p and ρ_w as shown in Figs. 11 and 14 are due to the different nature of each property. The effect of ε_p is acting throughout the packet of emulsion (distributed effect) whereas the effect of ρ_w is mainly acting at the boundary of the packet (local effect).

A check for the approximate but simple treatment of the scattering process in the radiative transfer is shown in Fig. 15. In the isotropic scattering approxi-

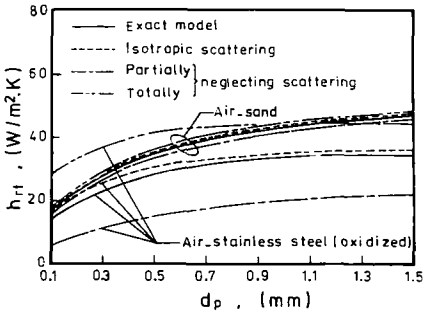

FIG. 15. Scattering approximations, $d_p = 1.0$ mm, $T_b = 600$°C, $W = 4$, oxidized copper surface, $T_w = 100$°C.

mation the phase function $p(\mu, \mu')$ was simply replaced by unity. With partial neglect of scattering, the scattering gain was neglected while keeping its attenuation effect. With total neglect of scattering both the gain and attenuation due to scattering were omitted. As shown in Fig. 15 the isotropic scattering approximation agrees well with the exact model for air–sand system, while exhibiting small overestimation for air–oxidized stainless steel system. This is because the isotropic scattering contributes more to the radiative flux in the forward direction toward the surface compared with the predominantly backward one of the exact solution. The other approximations agree well with the exact solution for air–sand system while fail for the other system. The conductive heat transfer coefficient h_c was not affected much by the different scattering approximations.

A check for gray medium approximation was made for air–sand and air–oxidized stainless steel having different spectral emissivity distributions, at different bed temperatures. In the gray medium approximation, the real surface and packet medium are treated as equivalent gray media having mean bulk radiative properties, obtained in terms of the corresponding spectral values by appropriate expressions [26]. It was found that the results for the gray medium approximation agree well with the results of the exact solution for all cases within an error not exceeding 5%. Usually the gray medium approximation can be applied for optically thick ($\tau_1 > 1$) packet layers even with remarkable spectral variation of the radiative properties [26]. This is the situation for many fluidized bed applications ($\tau_1 > 3$).

5. CONCLUSIONS

The present study proposes a model of bed to wall heat transfer in a high temperature fluidized bed which includes both conductive–radiative transfer from the emulsion packet and the radiative transfer from bubbles. The analysis of the radiative transfer in the emulsion is based on the assumption of the most real and practical systems in engineering and technology for which emission, absorption and scattering are considered. The semi-numerical solutions for both energy and radiative transfer equations are presented and applied to predict heat transfer coefficients for different fluidized bed systems with various operating conditions and bed characteristics. Comparisons are made with available experimental data and predictions by other analytical models in the literature. The main conclusions of the present study are:

(1) The predictions by the present analysis agree well with the available experimental results for different fluidized bed systems and heat transfer surfaces under various operating conditions.
(2) The relative radiative contribution of the overall heat transfer coefficient is appreciable (as much as 35%) for large values of bed particle diameter and emissivity, surface and bed temperatures, surface emissivity, and varies directly with them.
(3) The overall heat transfer coefficient is little influenced by the surface emissivity which exhibits nearly a maximum value at an optimum fluidizing velocity $U_o = 2U_{mf}$.
(4) The radiative contribution of the bubble phase is substantial for large fluidizing velocities, and surface and bed particle emissivities.
(5) The overall heat transfer coefficient would be noticeably affected by the variation in the thermal conductivity of the bed material for values of $k_s < 10\ \mathrm{W\ m^{-1}\ K^{-1}}$.
(6) For most practical applications the isotropic scattering approximation is acceptable. However, neglecting the scattering contribution (totally or partially) may lead to many errors with highly reflecting bed particles.
(7) The gray medium approximation can be accurately utilized for many practical fluidized bed applications with $d_p < 1.5$ mm where the condition of optically thick packet layer exists.

REFERENCES

1. J. S. M. Botteril, *Fluidized Bed Heat Transfer*. Academic Press, New York (1975).
2. S. C. Saxena and J. D. Gabor, Mechanisms of heat transfer between a surface and a gas fluidized bed for combustor application. *Prog. in Energy and Combustion Science* **7**, 73–102 (1981).
3. H. M. Shafey, L. T. Fan, A. A. Abdellatif, A. S. Huzayyin and I. M. S. Taha, Clean heat and power generation and energy saving using fluidized bed technology, Grant FRCU-830216, Egyptian–American Linkage Projects, reports No. 1 and 2, Assiut, Egypt, (1984).
4. V. N. Vedamurthy and V. M. K. Sastri, An analysis of conductive and radiative heat transfer to the walls of fluidized bed combustors. *Int. J. Heat Mass Transfer* **17**, 1–9 (1974).
5. K. Yoshida, T. Ueno and D. Kunii, Mechanism of bed wall heat transfer in a fluidized bed at high temperatures. *Chem. Engng Sci.* **29**, 77–82 (1974).
6. R. H. Thring, Fluidized bed combustor for the Stirling engine. *Int. J. Heat Mass Transfer* **4**, 911–918 (1977).
7. S. C. Bhattacharya and D. Harrison, Heat transfer in high temperature fluidized beds. *Proceedings of European Congress on Particle Technology, Nuremburg*, p. 23, Session K2 (1977).
8. A. K. Kolar, N. S. Grewal and S. C. Saxena, Investigation of radiative contribution in a high temperature fluidized-bed using the alternate-slab model. *Int. J. Heat Mass Transfer* **22**, 1695–1703 (1979).
9. He-Cheng Zhang, Ke-Fa Cen, Chen-Long Xie and Guo-Quan Huang, The analysis and experiment of immersed tube heat transfer in fluidized bed combustion boiler. *Proceedings of the 4th Int. Conference on Fluidization, Kashikajima, Japan*, p. 819, 29 May–3 June (1983).
10. G. Flamant et G. Arnaud, Analyse et modelisation du transfert de chaleure entre une paroi et un lit fluidise à haute température. *Int. J. Heat Mass Transfer* **27**, 1725–1735 (1984).
11. G. Flamant and T. Menigault, Combined wall-to-fluidized bed heat transfer. Bubbles and emulsion contributions at high temperature. *Int. J. Heat Mass Transfer* **30**, 1803–1812 (1987).

12. T. F. Ozkaynak, J. C. Chen and T. R. Frankenfield, An experimental investigation of radiation heat transfer in high temperature fluidized bed, *Proceedings of the 4th Int. Conference on Fluidization, Kashikajima, Japan*, p. 371, 29 May–3 June (1983).
13. Qian Renzhang, Huang Wendi, Xu Yunsheng and Liu Dechang, Experimental research of radiative heat transfer in fluidized beds, *Int. J. Heat Mass Transfer* **30,** 827–831 (1987).
14. N. Achara, M. E. Horsley, M. R. I. Purvis and R. H. Teague, Zonal heat transfer rates in a fluidized bed combustor, *Int. J. Heat Mass Transfer* **31,** 577–582 (1988).
15. S. Chandrasekhar, *Radiative Transfer*. Dover, New York (1960).
16. R. Siegel and J. R. Howell, *Thermal Radiation Heat Transfer*. McGraw-Hill, Kogokusha, Tokyo (1972).
17. T. Kunitomo, H. M. Shafey and T. Teramoto, Theoretical study on radiative properties of a painted layer containing spherical pigment (case of normal incidence), *Bulletin of the JSME* **22,** 1587–1594 (1979).
18. H. M. Shafey, I. S. Taha and A. S. Huzayyin, Computer-aided simulation of fluidized bed combustor, *Proceedings of the ASME 1989, Winter Annual Meeting, Analysis and Design of Energy Systems: Computer-Aided Engineering*, Vol. 10-1 pp. 43–52. ASME United Engineering Center, New York (1989).
19. C. L. Tien, Thermal radiation in packed and fluidized beds, *Trans. ASME, J. Heat Transfer* **110,** 1230–1242, (1988).
20. J. K. Parrot and A. D. Stuckes, *Thermal Conductivity of Solids*. Pion, London (1975).
21. Y. S. Touloukian, P. E. Liley and S. C. Saxena, *Thermophysical Properties of Matter*, Vol. 2. IFI/PLENUM, New York (1970).
22. Y. S. Touloukian and D. P. Dewitt, *Thermophysical Properties of Matter*, Vol. 8. IFI/PLENUM, New York (1972).
23. M. N. Özisik, *Radiative Transfer and Interactions With Conduction and Convection*. Wiley, New York (1973).
24. H. H. Blau, Jr. and J. R. Jasperse, Spectral emittance of refractory materials, *Applied Optics* **3,** 281–285 (1964).
25. A. M. Abd El-Ghany, Investigation of heat transfer between a surface and a gas-fluidized bed at high temperature, M.Sc. Thesis, Assiut University, Assiut, Egypt, (1992).
26. T. Kunitomo, M. Fujita and H. M. Shafey, The effect of paint coating on heat transfer, *Trans. JSME* (in Japanese) **50,** 839–844 (1984).